Characterization of high-Q optical microcavities using confocal microscopy

Rajan P. Kulkarni,[1] Scott E. Fraser,[1] and Andrea M. Armani[2,*]

[1]*Division of Biology, M/C 139-74 California Institute of Technology, Pasadena, California 91125, USA*
[2]*Mork Family Department of Chemical Engineering and Materials Science, University of Southern California, Los Angeles, California 90089, USA*
**Corresponding author: armani@usc.edu*

Received June 2, 2008; revised October 24, 2008; accepted October 25, 2008;
posted October 28, 2008 (Doc. ID 96876); published December 4, 2008

Confocal microscopy was initially developed to image complex circuits and material defects. Previous imaging studies yielded only qualitative data about the location and number of defects. In the present study, this noninvasive method is used to obtain quantitative information about the Q factor of an optical resonant cavity. Because the intensity of the fluorescent signal measures the number of defects in the resonant cavity, this signal is a measure of the number of surface scattering defects, one of the dominant loss mechanisms in optical microcavities. The Q of the cavities was also determined using conventional linewidth measurements. Based upon a quantitative comparative analysis of these two techniques, it is shown that the Q can be determined without a linewidth measurement, allowing for a noninvasive characterization technique.

OCIS codes: 100.2960, 100.4290, 120.4630, 120.6660, 180.1790, 230.5750.

Confocal microscopy was first described almost 50 years ago [1]. One of the first practical applications of reflection confocal microscopy was imaging semiconductor chips and flip-chip devices [2]. Confocal microscopy is especially suited for materials applications because of its ability to nondestructively create three-dimensional (3D) images of complex and highly intricate structures.

By integrating fluorescence into the detection, the biology community has obtained quantitative information using confocal microscopy, including the 3D structure of living cells [3] and receptor signaling pathways [4]. However, integrating fluorescence into a living sample is fairly straightforward. A previously unexplored alternative lies in exploiting the naturally occurring autofluorescence of the material. Certain materials, including silica, have an autofluorescence signal that can be excited under the appropriate conditions [5]. The autofluorescence results in a constant background signal from which the defects detract owing to scattering.

To demonstrate the utility and practicality of this technique, it was applied to characterizing the Q factor of planar arrays of ultra-high-Q microtoroid resonators [Fig. 1(a)]. These devices were fabricated as previously described in [6]. The laser reflow process on several devices was performed incorrectly intentionally, resulting in low Q factors and defects at the toroid periphery.

The microtoroids were imaged on an upright Zeiss 510 confocal microscope using a $20\times/0.5$ NA dry objective. The autofluorescence of silica was excited using a 488 nm argon laser. The data were taken using a 488 nm dichroic mirror and LP 505 filter in the light path, and the images were captured using the photomultiplier tube supplied with the microscope, with no subsequent processing. For these experiments, the pinholes were adjusted to obtain optical sections (Z) of $5-7$ μm in depth; the toroid minor diameter is approximately $5-7$ μm. To verify that the structure seen in the images resulted from the reflow process, confocal images were taken of the microdisk structure [Fig. 1(b).].

The Q factor of the resonator was determined using a narrow-linewidth tunable laser centered at 1550 nm[6]. Tapered optical fibers were used to excite resonant modes of the cavity (in the undercoupled regime), and the intrinsic modal linewidth (and hence intrinsic Q) was computed using a resonator-waveguide coupling model [7].

The resonant linewidths are shown in Figs. 2(a), 2(d), 3(a), and 3(d), respectively. The ultra-high-Q resonances in Figs. 2(a) and 2(d) correspond to Q factors of 1.68×10^8 and 2.25×10^8 while the low-Q resonances in Figs. 3(a) and 3(d) correspond to Q factors of 1.39×10^7 and 4.81×10^6. While these Qs are large in comparison to other resonant cavities, such as photonic crystals [8,9], polymer microresonators [10,11], and microdisks [12,13], which have yet to achieve $Q>5\times10^6$, they are low for toroid devices, which typically average above 1×10^8.

In the confocal micrographs, the fidelity of the toroid can easily be determined by examining the autofluorescence and scattering from the edge. In a correctly reflowed toroid, there are thin concentric

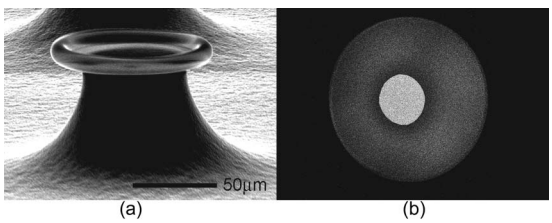

Fig. 1. (a) Scanning electron microscopy (SEM) image of an array of microtoroid resonators. (b) Confocal image (raw data) of the silica microdisk. It is important to note that the microdisk is fairly uniform in intensity. The highly reflective center region is the silicon pillar.

0146-9592/08/242931-3/$15.00

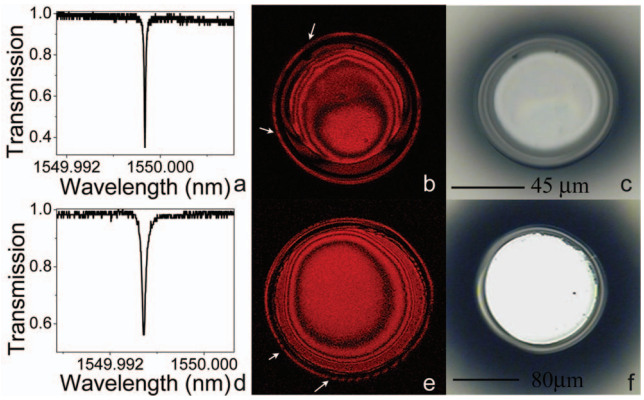

Fig. 2. Comparative characterization of two ultra-high-Q devices. (a) Resonant frequency with $Q=1.68\times10^8$. (b) Confocal and (c) reflection micrograph of device. (d) Resonant frequency with $Q=2.25\times10^8$. (e) Confocal and (f) reflection micrograph of device.

circular rings centered on the silicon pillar. Scattering from inhomogeneities resulted in dark areas within these rings. These rings were easily visualized [Figs. 2(b) and 2(e)] and are indicative of a $Q>10^8$. In lower Q toroids, these rings became increasingly fragmented and striations were seen at large angles, often perpendicular to the pillar [Figs. 3(b) and 3(e)]. As the Q decreased from 10^7 to 10^6, the number and size of the striations increased. Additionally, it is important to note that the location and the orientation of the striations are important in this application, because the optical mode of the resonator is located in the periphery of the microtoroid. Therefore, defects in this region will have a greater negative impact on the Q factor of the device than those located far from this region. For comparison, images were also taken using traditional bright-field or reflection microscopy [Figs. 2(c) and 2(f) and Figs. 3(c) and 3(f)]. Note that in these images, the low-Q and high-Q devices look relatively similar.

To quantify these images, the area that appears as nonautofluorescent (NA) in the image was calculated. To compare toroids of different sizes, this value was normalized by dividing it by the total two-dimensional (2D) area of the toroid (A_{toroid}); this expression shows the proportion of the surface that is nonautofluorescent (P). For example, if the entire toroid surface is autofluorescing, then $P=0/A_{\text{toroid}}=0$. However, if there were two dark regions (NA_1 and NA_2), then $P=(NA_1+NA_2)/A_{\text{toroid}}$. Therefore, as the number of black regions increased, P increased with a maximum value of 1.

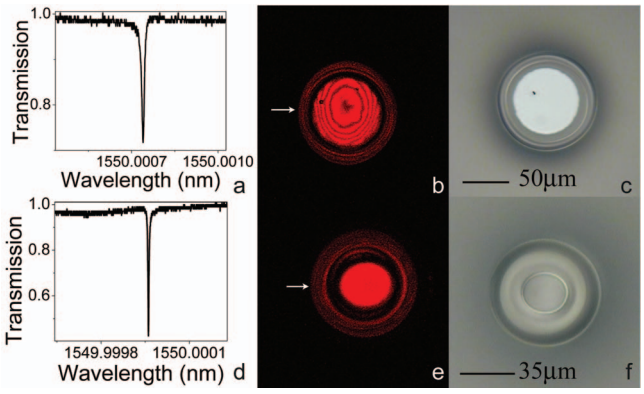

Fig. 3. Comparative characterization of lower Q devices. (a) Resonant frequency with $Q=1.39\times10^7$. (b) Confocal and (c) reflection micrograph of device. (d) Resonant frequency with $Q=4.81\times10^6$. (e) Confocal and (f) reflection micrograph of device.

By calculating the percentage of the total toroidal surface area encompassed by these dark regions, these images can be quantified and compared to the Q of the toroid. The characteristic equation for Q_{tot} is given by $Q_{\text{tot}}^{-1}=Q_{\text{ss}}^{-1}+Q_{\text{cont}}^{-1}+Q_{\text{mat}}^{-1}+Q_{\text{rad}}^{-1}+Q_{\text{coupl}}^{-1}$ [14], where Q_{ss} is the loss due to surface scattering, Q_{cont} is the loss due to contaminants on the surface, Q_{mat} is the material loss, Q_{rad} is the radiative loss, and Q_{coupl} is the coupling loss. Previous research with microtoroids and microspheres using tapered fiber waveguides at 1550 nm has shown that Q_{cont} and Q_{ss} are the dominant loss mechanisms [15]; therefore, this equation can be simplified to contain only the first two terms, Q_{cont} and Q_{ss}. Q_{cont} at 1550 nm is believed to result from adsorption of water molecules to the surface of the resonator and limits the Q value to the mid 10^8 range [14]. In a correctly fabricated toroid, Q_{ss} is a negligible contributor to Q for values in this range. The expression for Q_{ss} is [14]

$$Q_{\text{ss}}=\frac{\lambda^2 D}{2\pi^2\sigma^2 B},$$

where λ is the wavelength, D is the toroid major diameter, σ is the rms size of surface inhomogenities, and B is the correlation length. If the silica reflow is imperfect, then there can be irregularities at or near the surface that can lead to surface roughness or scattering within the volume of the resonant mode itself (owing to index variations). In this regime, Q_{ss} becomes the dominant loss mechanism.

When plotting Q_{tot} against the percentage of dark area in the toroidal region, as seen in Fig. 4, there is an identifiable trend that can be approximately fit to a function of the form $y=ax^b$. A fit yields $b=-0.49486$ and suggests an interpretation of the fractional area. In particular, we would expect this square-root relation between this area and an effective scattering length. We note, however, the exact nature of the defects is not presently known.

We have observed an empirical relation between the fractional area comprised of the dark bands area in the images and the measured Q factor. The dark bands are believed to result from scattering centers, surface inhomogeneities, or both that result during the improperly applied reflow process. Using this calibration, it is now possible to determine the Q of additional toroids solely by confocal microscopy. While we have used this method to characterize optical resonators, it can be expanded across many disciplines because most materials have some degree of autofluorescence [5]. This technique will provide an alternative method of determining quantitative information about device performance in fields as diverse

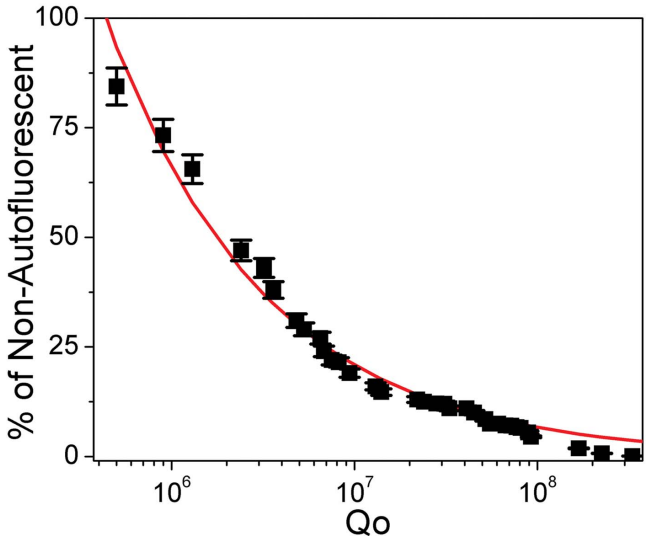

Fig. 4. (Color online) As the percentage of scattered light in the toroid decreases, the Q factor increases. This increase in Q is directly related to the decrease in the number and size of surface inhomogeneities. The curve is the fit to the experimental results, based on the theoretical framework outlined.

as quantum computing [16], polymer electro-optic devices [17], optical sensors [18], and solar cells [19].

This work was supported at the California Institute of Technology at the Beckman Imaging Center and by the University of Southern California by the Program on Women in Science and Engineering (WISE) and the Provost's Initiative on Biomedical Nanoscience.

References and Notes

1. In confocal microscopy, images are generated through the use of pinholes, which selectively capture light from the in-focus section of the illuminated image. The fluorescent light returning to the objective includes both fluorescence from the optical section in focus as well as other depths of the sample. The pinhole size can be expanded to allow more light in or it can be narrowed to restrict light. By reducing the size of the pinhole, light from shallower or deeper sections (relative to the optical section in question) can be rejected, thus allowing for imaging of a very thin depth of the sample.
2. T. Wilson, J. N. Gannaway, and P. Johnson, J. Microsc. **118**, 309 (1980).
3. B. Bailey, D. L. Farkas, D. L. Taylor, and F. Lanni, Nature **366**, 44 (1993).
4. D. S. Lidke, P. Nagy, R. Heintzmann, D. J. Arndt-Jovin, J. N. Post, H. E. Grecco, E. A. Jares-Erijman, and T. M. Jovin, Nat. Biotechnol. **22**, 198 (2004).
5. A. J. Nijdam, M. M. C. Cheng, D. H. Geho, R. Fedele, P. Herrmann, K. Killian, V. Espina, E. F. Petricoin, L. A. Liotta, and M. Ferrari, Biomaterials **28**, 550 (2007).
6. D. K. Armani, T. J. Kippenberg, S. M. Spillane, and K. J. Vahala, Nature **421**, 925 (2003).
7. M. Cai, O. Painter, and K. J. Vahala, Phys. Rev. Lett. **85**, 74 (2000).
8. K. Srinivasan and O. Painter, Opt. Express **10**, 670 (2002).
9. Y. Takahashi, H. Hagino, Y. Tanaka, B. S. Song, T. Asano, and S. Noda, Opt. Express **15**, 17206 (2007).
10. A. M. Armani, A. Srinivasan, and K. J. Vahala, Nano Lett. **7**, 1823 (2007).
11. C. Y. Chao and L. J. Guo, J. Vac. Sci. Technol. B **20**, 2862 (2002).
12. M. Soltani, S. Yegnanarayanan, and A. Adibi, Opt. Express **15**, 4694 (2007).
13. K. Srinivasan, M. Borselli, and O. Painter, Opt. Express **14**, 1094 (2006).
14. M. L. Gorodetsky, A. A. Savchenkov, and V. S. Ilchenko, Opt. Lett. **21**, 453 (1996).
15. T. J. Kippenberg, S. M. Spillane, and K. J. Vahala, Appl. Phys. Lett. **85**, 6113 (2004).
16. B. Dayan, A. S. Parkins, T. Aoki, E. P. Ostby, K. J. Vahala, and H. J. Kimble, Science **319**, 1062 (2008).
17. P. Rabiei, W. H. Steier, C. Zhang, and L. R. Dalton, J. Lightwave Technol. **20**, 1968 (2002).
18. A. M. Armani, R. P. Kulkarni, S. E. Fraser, R. C. Flagan, and K. J. Vahala, Science **317**, 783 (2007).
19. T. Buonassisi, A. A. Istratov, M. A. Marcus, B. Lai, Z. H. Cai, S. M. Heald, and E. R. Weber, Nature Mater. **4**, 676 (2005).